JAAS

Time-resolved imaging of atoms and molecules in laser-produced uranium plasmas

Journal:	*Journal of Analytical Atomic Spectrometry*
Manuscript ID	JA-ART-07-2019-000228.R1
Article Type:	Paper
Date Submitted by the Author:	20-Aug-2019
Complete List of Authors:	Kautz, Elizabeth; Pacific Northwest National Laboratory, National Security Directorate Skrodzki, Patrick; University of Michigan, Nuclear Engineering and Radiological Sciences; University of Michigan, Gerard Mourou Center for Ultrafast Optical Science Burger, Milos; University of Michigan, Nuclear Engineering and Radiological Sciences; University of Michigan, Gerard Mourou Center for Ultrafast Optical Science Bernacki, Bruce; Pacific Northwest National Laboratory Jovanovic, Igor; University of Michigan; University of Michigan, Gerard Mourou Center for Ultrafast Optical Science Phillips, Mark; University of Arizona, Optics Science Center; Opticslah; Pacific Northwest National Laboratory, National Security Directorate Harilal, Sivanandan; Pacific Northwest National Laboratory, Applied Physics

ARTICLE

Time-resolved imaging of atoms and molecules in laser-produced uranium plasmas

Received 00th January 20xx,
Accepted 00th January 20xx

DOI: 10.1039/x0xx00000x

E. J. KAUTZ,[a] P. J. SKRODZKI,[b,c] M. BURGER,[b,c] B. E. BERNACKI,[a] I. JOVANOVIC,[b,c] M. C. PHILLIPS,[a,d,e] S. S. HARILAL[a,†]

Gas-phase oxidation of uranium (U), plume chemistry, and the corresponding impact on optical emission features of the U plasma are investigated. Plasmas were produced via nanosecond laser ablation of a natural U target in a chamber where U oxidation was controlled by varying the oxygen partial pressure in an argon cover gas. Monochromatic imaging of U atoms and monoxide (UO) molecules was performed using narrow bandpass optical filters. Results reveal the spatio-temporal evolution of atomic and molecular species in the plasma. U oxides are found to be formed further from the target (in comparison to U atoms), where lower temperatures favor molecular recombination. Segregation between the distribution of U atoms and UO species is observed at later times of plasma evolution, and is more apparent at lower oxygen partial pressures. At higher oxygen partial pressures, significant variation in plume morphology is noticed for UO species, which can be attributed to the higher oxide (U_xO_y) formation further from the target. The monochromatic images of U atoms and UO molecules and corresponding spectral features at various oxygen partial pressures presented here provide unique insight into gas-phase, high-temperature U oxidation and chemistry, with implications for a wide range of nuclear applications, from stand-off detection of radioisotopes to forensics and safeguards.

I. Introduction

Physical and chemical processes within uranium (U) plasmas present an essential aspect of accurate nuclear forensic analysis, with implications for several application areas ranging from nuclear fuel fabrication, reactor diagnostics, environmental monitoring, to safeguards and security.[1-7] Laser-produced U-containing plasmas can be used as a testbed for developing an understanding of fireball plasma chemistry and combustion events, generation of particulates and debris in an explosive event or accident scenario, and to generate input for modeling tools.[8, 9] Further, the analysis of laser-produced plasmas (LPP) via optical spectroscopy is a well-established approach for elemental and isotopic detection of U-bearing materials, even at stand-off distances.[10-12]

Gas-phase U oxidation and corresponding plasma chemistry are very complex.[13, 14] Recent studies investigated the chemical pathways in which atomic U species react with oxygen species to form U oxides in LPPs.[8, 15-20] U oxide formation mechanisms are strongly influenced by the physical conditions of the plume (e.g. temperature, density) as well as the number density of oxygen molecules available for oxidation.[8, 15, 20-22] The reaction mechanisms leading to the formation of U_xO_y are very complex and involve numerous reaction channels, leading to the formation of several oxide species (e.g. UO, UO_2, UO_3, U_2O_3, U_2O_2).[23] Such molecular species are believed to be precursors for nano- and micro-clusters in a LPP or fireball.[24-28] Hence, the formation of higher gas-phase U oxide molecules (e.g. UO_2, UO_3, more generically referred to as U_xO_y) in the LPP is an intermediate step in the formation of aggregated nanoparticles via coalescence of molecules.[28, 29]

[a] Pacific Northwest National Laboratory, Richland, WA 99352 USA
[b] Department of Nuclear Engineering and Radiological Sciences, University of Michigan, MI 48109 USA
[c] Gérard Mourou Center for Ultrafast Optical Science, University of Michigan, MI 48109 USA
[d] Optics Science Center, University of Arizona Tucson, AZ 85721 USA
[e] Opticslah, LLC, Albuquerque, NM 87106 USA
† Corresponding author: hari@pnnl.gov
See DOI: 10.1039/x0xx00000x

Although some studies exist in the literature,[7, 8, 10, 15, 16, 23] there is presently a lack of comprehensive understanding of chemical pathways and physical conditions that lead to higher gas-phase U oxide formation, including *when and where* such molecules are formed in a transient LPP plume. Optical emission spectroscopy (OES) of LPPs, commonly referred to as laser-induced breakdown spectroscopy (LIBS), provides a sensitive, non-invasive diagnostic tool for investigation of U-containing plasmas.[10, 30] Optical spectroscopy of atomic species in a laser-produced plasma is routinely used for isotopic analysis.[10] Molecular LIBS measurements is also a powerful tool for detecting isotopic shifts.[10, 18, 31, 32]

Several prior studies have investigated U and UO emission using OES.[8, 17-20] Most of these studies have been carried out either in a space-integrated manner or using line-of-sight measurement. While such studies provide important insight into U plasma chemistry, OES alone cannot give details about the complex morphological behavior of the plasma and its constituents. Fast-gated imaging allows for direct observation of plume morphology in a spatially- and time-resolved manner. Imaging of the LPP plume provides important information that is complementary to OES, including species distribution and segregation, plume expansion, confinement, instabilities, and persistence.[10] Previous studies employed filtered (monochromatic) imaging for tracking molecular formation (e.g. AlO[33, 34], CN[35] etc.) in LPPs. Other information such as plume velocity, shape, shock wave propagation, and temperature distribution can also be elucidated from plasma plume imaging.[15, 22, 36-40] Combining OES with plasma imaging via narrow-band filters allows direct measurement of spatio-temporal distribution of various species in the LPP.

In the present work, we investigate distributions of atomic and molecular U species in a controlled reactive environment in order to better understand how oxidation impacts LPP morphology and emission. The monochromatic images of U atoms and molecules and corresponding spectral features presented here provide unique insight into gas-phase U chemistry, U atomic and UO/U_xO_y molecular formation physics, with implications for improved understanding of debris generation pathways typical of a combustion event.

II. Experimental details

Figure 1 shows the experimental set-up used for OES and fast gated monochromatic imaging using narrow bandpass filters. A Nd:YAG laser (1064 nm, 6 ns full-width half-maximum (FWHM)) was used to produce U plasmas. This laser was focused normal to a U metal target (with natural isotopic abundance) using an anti-reflection coated plano-convex lens with a focal length of 15 cm. Laser power density at the target material was ~ 2 GW/cm^2, corresponding to a laser energy of ~90 mJ, with a spot size of ~1 mm. The target was mounted in a vacuum chamber which contains optical windows for laser ablation and light collection, vacuum ports for gas feed-through (for environmental control), and pressure gauges. A custom-built gas manifold, which contains gauges and several leak valves, was used for controlling the gas feed-through to the chamber. This vacuum chamber was placed on an *x-y-z* translator so that different regions of the target could be exposed for preventing target drilling. The use of this vacuum chamber also allowed for any target particulate matter to be contained within the chamber.

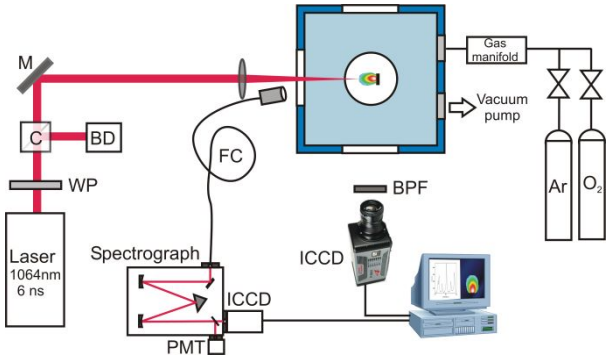

Fig. 1 Schematic of the experimental set-up used for collecting spectral information and imaging data. Acronyms in the schematic are defined as follows: WP-waveplate; C-cube; BD-beam dump; M-mirror; FC – fiber cable; ICCD – intensified CCD, BPF – bandpass filter.

The emission images presented in this work were collected by placing an intensified CCD (ICCD) camera (PI-MAX4, 1024×1024 pixels) orthogonal to the plasma expansion direction. A telephoto lens was used for imaging the self-emission from the plasma to the intensifier of the ICCD. Monochromatic imaging of U atomic and UO molecular species was performed by inserting narrow bandpass filters centered at 404 nm (bandwidth FWHM ~1 nm) and 593.5 nm (FWHM ~ 0.18 nm), respectively, in front of the camera. In addition to imaging, spatially-integrated OES was performed, where the light emitted from the U plasma was collected with a lens and focused to a 400 µm multimode fiber. The optical fiber was coupled to a 0.5 m Czerny-Turner spectrograph (Spectrapro 2500). An ICCD camera (Andor iStar) was used for detection which was synchronized with the laser pulsing via a delay generator. The spectrograph provided a spectral resolution ~0.04 nm, measured using a He-Ne laser, using 2400 grooves/mm grating. Acquisition gate delay and integration time were varied to allow for time-resolved measurements, both for emission imaging and spectral measurements. To capture the time-resolved U plasma evolution, filtered images were taken over a range of time delays with respect to the onset of plasma formation: 1-10 µs with 1 µs time steps between images, and 10 and 100 µs with 10 µs steps between images.

For controlling U plasma chemistry and oxidation, the partial pressure (PP) of oxygen gas (O_2) was varied from 1 to 20% in an argon (Ar) cover gas using the gas manifold. The inert Ar cover gas was chosen to isolate reaction pathways between U and O species. A total pressure of 100 Torr was used for all O_2 PPs tested here (1, 5, 10 and 20% O_2 PP). These PPs correspond to O_2 concentrations in the range of 3.2×10^{16} – 6.4×10^{17} cm^{-3}. The 100 Torr pressure was selected because it has been

previously reported to have nearly optimal signal-to-noise ratio for atomic emissions using ns-LIBS.[41] UO molecular formation can occur from interaction of target species with O_2 gas in the ambient (i.e. combustion), or O_2 impurities on the target surface. Since the target surface was cleaned of U oxides by firing a few shots of the laser prior to data collection, we assume the interaction between target and ambient species is the dominant mechanism for UO and higher oxide formation.

III. Results & Discussion

a. Uranium and Uranium Oxide Spectroscopy

OES of U plasma plumes reveals the atomic and molecular emission features and plasma persistence. In a LPP, the emission from atoms and ions is dominant at the earliest times, while the molecular emission appears at later times during plasma evolution when the temperatures are lower.[10] The favored physical conditions for UO formation occur in the temperature range ~1500–5000 K.[42] The delayed appearance of molecular emission in ns-LPP is due in part to the presence of strong shock waves, as well as higher temperatures at the early times of the ns-LPP.[33, 42] OES spectral features were collected at varying O_2 PPs (1, 5, 10, and 20%). Figure 2 shows representative spectral features in the wavelength range of 591-595 nm for each O_2 PP. All spectra shown in the present work are spatially-integrated. U, UO, and higher oxide (U_xO_y) lines exist in the spectral window given in Figure 2(a), which were all taken at the same delay time of 15 µs and gate width of 5 µs, so that intensities of each peak can be directly compared. The prominent spectral features seen in Figure 2(a) are labeled for 1% O_2 PP and include the U I resonance transition at 591.54 nm (0–16900 cm^{-1}), the near-resonance line at 593.38 nm (620–17468 cm^{-1}), and a broader spectral feature of UO peaked at 593.55 nm. A strong background-like emission is apparent in the spectral features which could be related to U_xO_y.[42]

The spectral features given in Figure 2(a) show significant variation in the intensities of U and UO for varying O_2 PPs, even with similar gate delays and widths. This result indicates that oxidation chemistry impacts spectral emission features. Our recent studies highlighted the presence of oxygen in the environment during U plasma expansion leads to a reduction in both excited and ground states populations of U atomic emission, and the persistence of such species.[16, 42] Figure 2(b) provides the U I (591.54 nm) and UO (593.55 nm) persistence with respect to O_2 PP measured using optical time-of-flight.[43] The persistence of U plasma emission was found to be ≥ 60 µs with 1% O_2 PP and it was reduced to ≤ 30 µs with the introduction of 10% O_2 PP and greater.[42] Figure 2(a) shows that at lower O_2 PPs the emission from U I dominates, whereas at higher O_2 PPs, the UO peak at 593.55 nm becomes the most prominent emission. When emission from UO dominates, atomic U I lines emanating from higher excited levels disappear. For example, at 1% O_2 PP the UO peak is found to be weaker, while at 20% PP, the major peaks are UO at 593.55 nm and U I resonance line at 591.54 nm. The reduction and enhancement of U I and UO spectral emission with increasing O_2 PPs can be

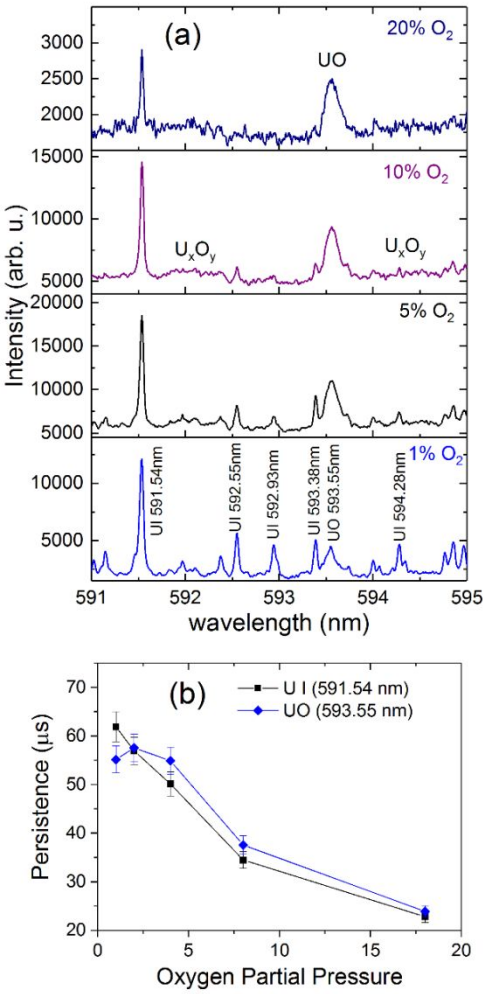

Fig. 2 (a) U I and UO spectral features recorded at 100 Torr pressure with a gate delay 15 µs and gate width of 5 µs for O_2 PP in the range of 1–20%. All measurements were taken in a space-integrated manner. (b) Persistence versus oxygen partial pressure for U I and UO peaks at 591.54 nm and 593.55 nm, respectively.[43]

related to oxidation in the plasma plumes, which occurs when the temperature of the plasma is lower and sufficient number density of oxygen molecules is present.

Since similar conditions were used for all measurements (e.g. laser irradiation, detection), with the exception of changing O_2 PP, we can conclude that plasma chemistry is the major reason for the reduction in emission intensity and persistence of all species in the plume. The spectral measurements given in Figure 2(a) were measured in a space-integrated manner. However, the LPP source is an inhomogeneous system where the temperature of the plasma varies significantly with distance from the target,[10] which may affect the locations of molecular formation within the plasma

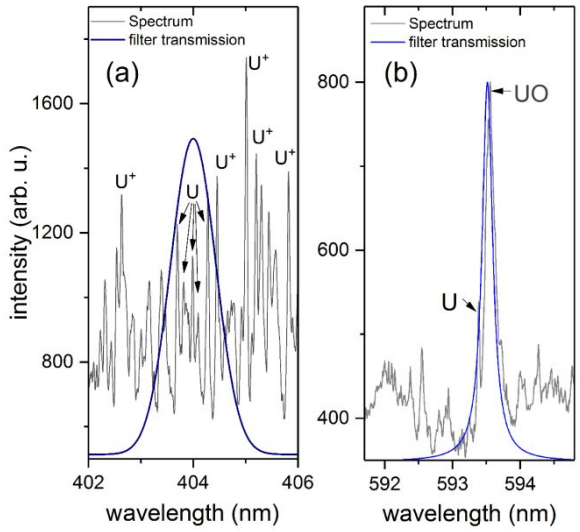

Fig. 3 Transmission curves of the narrow bandpass filters used for monochromatic imaging with spectral features recorded at 5% O_2 PP for: (a) 404 nm filter with 1 nm FWHM, with U spectral features recorded at a delay time 1 μs and 1 μs gate width, and (b) filter transmission profile peaked at 593.5 nm with 0.18 nm FWHM with UO spectral features at 593.55 nm recorded at delay time 20 μs and 20 μs gate width.

plume. Hence, monochromatic imaging of U and UO is performed to provide additional, and valuable, insight into plasma chemistry.

b. Monochromatic Imaging of atoms and molecules

Fast-gated imaging gives insight into morphology and evolution of plasma plumes. Such diagnostics are needed to improve understanding of the interaction between the U plasma plume and the surrounding oxygen-containing atmosphere. Narrow-band imaging of excited populations of U atomic and molecular species in the plume gives detailed information on the spatio-temporal distribution of atoms and molecules which act as precursors to higher U oxides and nanoparticles. The transmission bandwidths of the narrow-band filters used for imaging and the representative emission in this spectral range from U LPPs are provided in Figure 3. The filters selected for this work isolate emission features originating from atomic U as shown in Figure 3(a), and UO as shown in Figure 3(b). In Figure 3(a) it is clear that the U spectral features between 402 and 406 nm are very crowded, and the 404 nm filter was specifically selected to isolate the U I atomic emission. However, there is some overlap with U I atoms and U ions with the use of the 404 nm filter. In ns-LPPs, the ion emission persistence is limited to early times when hotter conditions exist in the plasma.[10] In the Figure 3(b) plot, we see that U and UO features are closely spaced in the crowded U spectra. For example, UO images may contain emission from the U I line at 593.38 nm at early times. At late times of plasma evolution, based on the spectral details given in Figure 2, it can be concluded that the recorded emission from the plasma is primarily due to UO. Using narrow bandpass filters described by Figure 3, time-resolved images of U atoms and UO molecules were collected for varying O_2 PP (1, 5, 10 and 20%).

Detailed high resolution spectroscopic and 2D spectral imaging studies were performed in prior work to investigate U and UO with varying O_2 PPs.[42, 43] Results from these studies highlighted that the atomic and molecular species predominate at early and late times of plasma evolution, respectively. While UO images recorded using the 593.5 nm bandpass filter at early times may contain emission from UI (peaked at 593.38nm), at later times of plasma evolution, images reported here are primarily contributed by emission from UO and U_xO_y species.

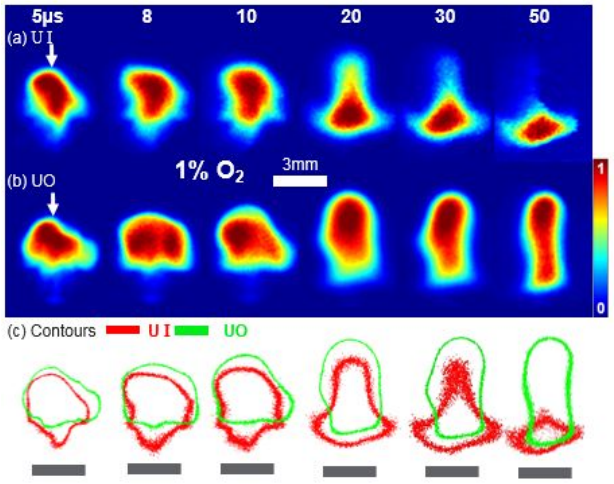

Fig. 5 Monochromatic, fast-gated imaging of a U plasma plume produced via ns-LA in 1% O_2 PP with an inert Ar cover gas in a total chamber pressure of 100 Torr. (a) U I images of the LPP taken with a 404 nm narrow bandpass filter, (b) UO images taken with a 593.5 nm bandpass filter, and (c) contours of U I and UO images. Each image is obtained from a single laser shot. All contours plotted are 25% of the maximum intensity of each image. The white arrows represent the incident laser direction, which is consistent for all plasma images presented. The grey rectangular boxes in (c) represent the target position. Each image given is normalized to its maximum intensity.

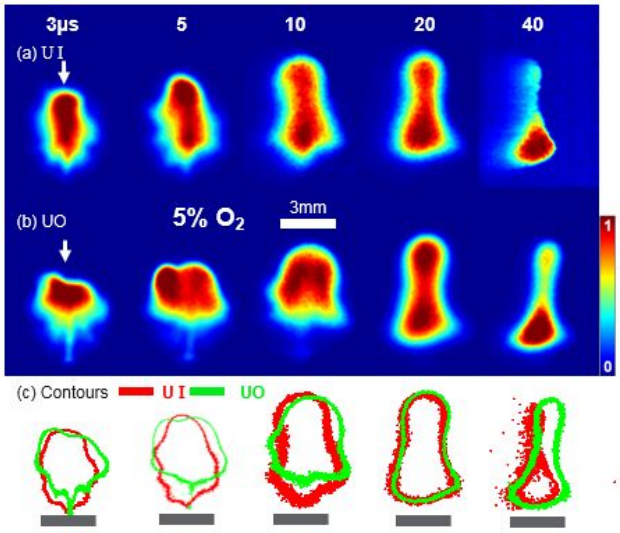

Fig. 6 Monochromatic, fast-gated imaging of (a) U I, (b) UO species and (c) contours for a U plasma plume produced via ns-LA in 5% O_2 PP with an inert Ar cover gas in a total chamber pressure of 100 Torr. Additional details are provided in the

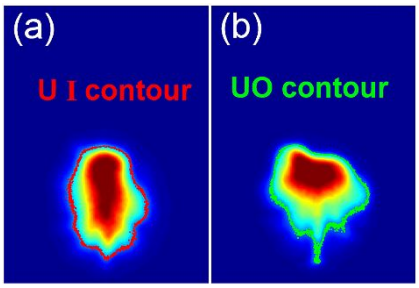

Fig. 4 Representative schematic showing contours plotted with corresponding (a) U I and (b) UO images. U plasma images shown here are for 5% O_2 PP at 3 µs delay time. Contours are plotted at 25% of the maximum intensity.

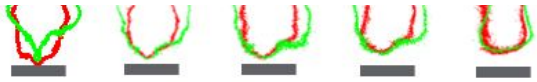

Fig. 7 Monochromatic, fast-gated imaging of (a) U I, (b) UO species and (c) contours for a U plasma plume produced via ns-LA in 10% O_2 PP with an inert Ar cover gas in a total chamber pressure of 100 Torr. Additional details are provided in the Figure 5 caption.

Raw grayscale images collected using these filters were processed by stretching (i.e. enhancing) contrast, sharpening (via high boost filtering), and smoothing (via Gaussian filtering) using MATLAB R2018a. Additionally, a false color-map was applied after image processing in order to emphasize intensity variations more clearly than are visible in grayscale. To account for large differences in absolute emission, image intensities were scaled for each image from 0 to 1. Contours of U I and UO images were generated from the processed images to visualize the distribution of atomic and molecular species in the plume. Here, contours are drawn at a level of 25% of the maximum intensity (unless otherwise noted) in each image. Examples of contours overlaid on U I and UO filtered images are provided in Figure 4 (a) and (b), respectively. Figure 4 illustrates how the contours presented in subsequent figures compare to plasma images. The contours can be used here to better understand how U I and UO species are spatially distributed within the plume, and their relative distance from the target. The value of 25% of the maximum intensity was chosen empirically as the contour boundary. A value of less than 25% resulted in a noisy boundary and was therefore not used.

U I and UO contours are presented with corresponding plasma images in Figures 5-8, where the direction of the incident laser beam is shown with an arrow, and the target position is indicated with small rectangles relative to contours plotted in (c). Several prior works reported spectrally-integrated images;[8, 44] however, since there are several molecular and atomic species emitting in the plume, additional diagnostic tools, such as optical time-of-flight (OTOF) spectroscopy,[16] are required in order to separate the spatio-temporal distributions of selected species in the plasma. The overlaid U I and UO contours presented in Figures 5-8 offer high spatial resolution (correspondent to resolution of the optical system, including camera and imaging optics). The results provided by monochromatic imaging and the corresponding image contours can be compared to modeling results previously reported for U plasmas.[15] Shot-to-shot variations due to presence of instabilities exist in the image data reported here cannot be avoided. Fluctuations were estimated at less than 8%.[42]

The time scales given in image sequences are different for various O_2 PPs to best illustrate the plume evolution, which varies based on the composition of the ambient gas. For example, the emission images are recorded for times ≥ 50 µs for 1% O_2 PP, while persistence is limited to ~20 µs for 20% O_2 PP. The reduction in the persistence of the plasma at higher O_2 PPs is due to enhanced oxidation within the plume. U I and UO morphologies are also found to vary with O_2 PP. When a U plasma expands in an oxygen-containing environment, different factors control the plume morphology, including the localized temperature and the availability of oxygen for reaction with species in the plume (e.g. U atoms, UO molecules). Our recent studies showed that initial excitation temperature in the plasma is similar, regardless of O_2 PP. However, temperature decreases more rapidly for higher O_2 PP environments, which is consistent with reported spectral features.[42]

At lower O_2 PPs, the monochromatic images of U I and UO show similar plume morphologies at early times (≤ 5 µs). This trend can be understood by evaluating the spectral features of U I and UO species at lower O_2 PPs (previously presented in Figure 2(a)), where the U I line at 593.38 nm dominates over UO. Although a narrow bandpass filter with ~ 0.18 nm FWHM is used in the present study, isolating UO from U atomic emission is not possible at lower O_2 PP and in the early stages of plasma evolution. Additionally, the broadband emission due to U_xO_y is present in all recorded images. This background is also seen

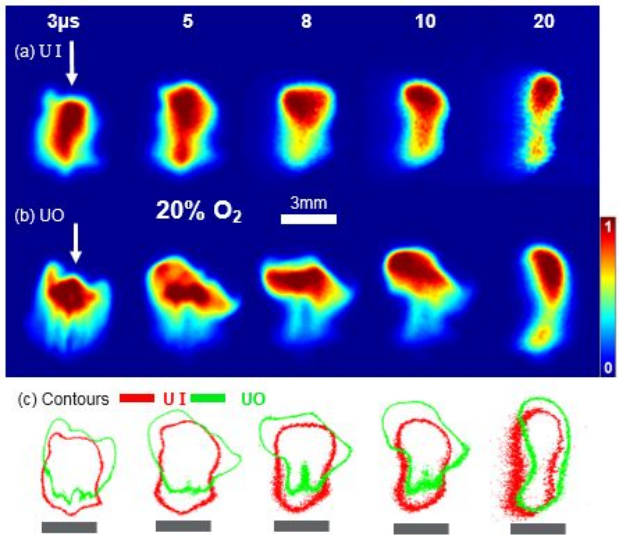

Fig. 8 Monochromatic, fast-gated imaging of (a) U I, (b) UO species and (c) contours for a U plasma plume produced via ns-LA in 20% O_2 PP with an inert Ar cover gas in a total chamber pressure of 100 Torr. Additional details are provided in the Figure 5 caption.

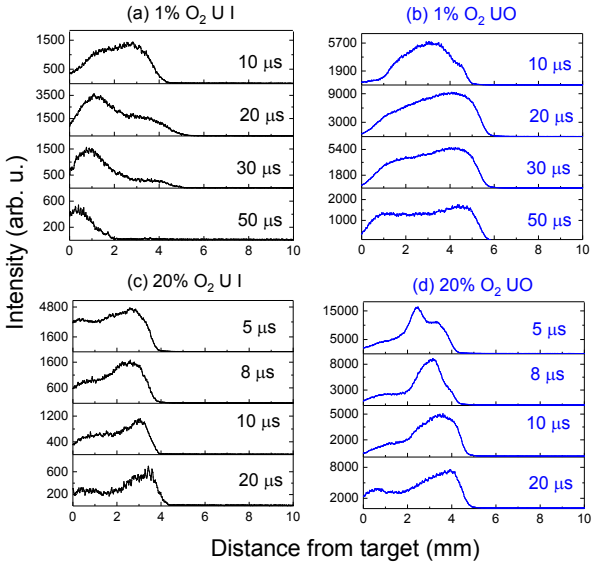

Fig. 9 Intensity versus distance from the target for: (a,b) 1 % O_2 PP U I and UO, respectively, and (c,d) 20% O_2 PP U I and UO. All data was collected at 100 Torr total chamber pressure in an inert Ar gas with the O_2 PP noted above. All plots are background corrected. The emission zone of the plasma analysed is shown in Figure 10 (e).

(and labeled) in the spectral features presented in Figure 2(a). At 1% O_2 PP, we observe a greater distinction in the spatial distributions of U I and UO species at later times at all O_2 PPs. At later times of plasma evolution, there is minimal U I emission detectable in the plasma plume and the main contribution to the emission is contributed by UO and background from higher oxides that were not specifically measured here.

Contours of monochromatic images given in Figure 5 show different emission zones for U I and UO, which are very clear at later times of plasma evolution. Contours show that UO emission is found to occur further from the target, in comparison to U I. There are also overlapping regions within these contours, particularly for the 5% O_2 PP case (Figure 6), indicating that UO still exists in the plume core with U I. The coexistence of UO and U I species agrees well with prior work that indicates U I and UO both react with oxygen gas that is transported towards the plume core to form higher oxides.[8, 15] Differences in plume morphology observed in plasma images and contours with varying O_2 PPs can be attributed to U oxidation thermo- and plasma chemistry changes that vary with O_2 PP. Plasma plume morphology is controlled both by temperature and availability of oxygen to react with U atomic and molecular species.[42]

The spatio-temporal distribution of U I and UO species observed in the monochromatic images can also be understood by analyzing the intensity counts obtained from the ICCD images along the plume expansion direction (normal to the target). Representative intensity versus distance plots for times corresponding to image data reported in Figures 5 and 8 are provided in Figure 9 (a) –(d) for 1% and 20% O_2 PP. From Figure 9 (a) and (b), we see that for the 1% O_2 PP, U I emission is strongest closer to the target, with U I and UO emission clearly segregated in space. For 20% O_2 PP, the U I and UO emission is not as distinctly separated in comparison to 1% O_2 PP, meaning U I and UO emission coexist. However, it can be seen from Figures 5-8 that the plume length is shortened considerably for 20% O_2 compared to 1% O_2 PP, suggesting that UO is consumed further from the target, leading to the formation of higher oxides (U_xO_y). With increasing O_2 PP, emission persistence of the plasma is limited to early times due to oxygen-assisted chemistry. Regardless of the O_2 PPs used, the UO emission originates further from the target, where lower-temperature conditions exist. Both the existence of lower temperatures and higher oxygen concentration further from the target promote oxidation.

The spatial distribution and dynamic behavior of the plume expansion in a cover gas with varying O_2 PPs given in Figures 5–8 can be used to generate U I, and UO spatio-temporal contour plots. Such plots provide another dimension to the fast gated and monochromatic imaging diagnostic tool, and give time-distance-intensity variations of atomic and molecular species in a concise plot. Figure 10 (a)–(d) presents representative space-time contour plots for 1% and 20% O_2 PPs. These plots were generated from image data collected using the narrow band-pass filters previously described. A sampling of such image data and the emission zone analyzed is shown in Figure 10(e). Space-time contour plots were made by first normalizing all raw image data for a given filter (404 nm or 593.5 nm) and time series (1-10 μs with 1 μs steps), and measuring the average pixel intensity in the emission zone. An emission zone ~0.34 mm wide was analyzed. All plots were normalized to the same intensity color scale, which is presented alongside space-time contour plots. As can be seen in Figure 10(a)–(d), UO species persist for longer relative to U I. Additionally, as O_2 PP increases, U I and UO

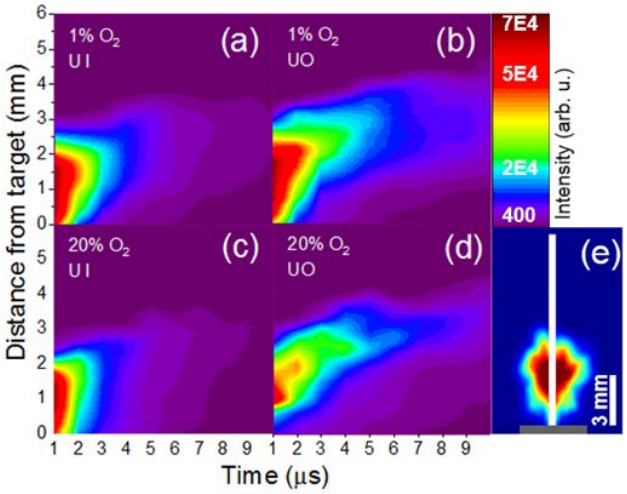

Fig. 10 Distance-time-intensity plots of U plasmas imaged using narrow bandpass filters for 1% and 20% O_2 PPs, where: (a) 1 % O_2 PP U I, (b) 1 % O_2 PP UO, (c) 20% O_2 PP U I, and (d) 20% O_2 PP. (e) Emission zone analysed (width of 0.34 mm) to generate plots.

persistence decreases, which is consistent with data previously reported in Figure 2(b).

The interaction between a high-Z (U) plume and a low-Z ambient gas (i.e. an ambient gas containing Ar or O_2) is complex, and this plasma-chemical interaction has previously been modeled.[15] While some models assumed the plume to be spherically symmetric,[45, 46] this assumption may be an over simplification considering the presence of instabilities in the plume-ambient interface during plasma expansion in a relatively high-pressure environment, such as that used in this study. The recorded plume images (Figures 5–8) show shot-to-shot fluctuations, although changes in intensities are ≤ 7%. Fluctuations are caused by the presence of Rayleigh-Taylor and Richtmyer-Meshkov instabilities.[44, 47] Finko and Cureli[15] reported the interplay between plasma-gas chemistry and plume dynamics in a U plasma in a simulated laser-plasma system. While our exact experimental conditions (e.g. pressure, O_2 PP, laser energy, laser pulse timing) differ from the parameters used in their simulation, the same evolutionary pathway of U and UO species in an oxygen-containing environment are observed.[15]

The spectral features and monochromatic images show a reduction in persistence for atomic and molecular species in the U plume with increasing O_2 PPs. Evolution of the U plume involves both turbulent transport of oxygen towards the plume core, and the reaction of U atomic species with oxygen leading to the formation of oxide species. Turbulent transport of oxygen and the reaction of U atoms with oxygen forms regions of the plasma with varying chemistry and temperature. Significant differences can be seen by comparing the monochromatic images and contours obtained with the lowest (1%) and the highest (20%) O_2 PPs. The U I and UO segregation in space is more evident with 1% O_2 PP. This segregation can be understood by considering the lower concentration of oxygen available for oxidation chemistry, which effectively increases the persistence of the plasma plume. The images also highlight the maximum intensity location of UO is moving towards the target at later times. This trend could be due to several reasons, including: (1) the oxygen transport to the plume core which reacts with U atomic species, and forms UO, (2) UO is formed further from the target and is consumed in the formation of higher oxides (U_xO_y), and (3) existence of lower temperatures near the target at later times of plume evolution. Changes in UO plume morphology are pronounced for higher O_2 PP of 20%, which can be seen in the lack of symmetry in the UO images. This observation can also be related to the formation of higher oxides and displacement of UO to outer regions of the plume.

In all O_2 PPs studied here, UO emission is present along with emission signal from higher oxides (e.g. UO_2, UO_3, U_2O_2, U_2O_3)[8, 16, 42] Several reaction mechanisms leading to the formation of such higher oxides[23] warrants further experimental investigation in order to compare proposed reaction mechanisms to modeling results.[15, 23] Imaging and diagnostic tools presented here (narrow bandpass filtering, image processing, image contours, and space-time contour plots) in conjunction with spectral measurements can be applied to future studies to investigate the chemical evolution and physical conditions associated with higher oxide evolution and spatial distribution within the plume.

IV. Conclusions

Here, we investigated the evolution of ns-laser produced U plasmas in the presence of varying O_2 PPs using OES and monochromatic fast-gated imaging. Narrow bandpass filters were employed to perform monochromatic imaging of U atoms and UO molecules in the plasma. Imaging at varying O_2 PPs (1-20%) in an Ar cover gas at 100 Torr pressure reveals that U atoms and UO molecules are segregated in space, and UO exists at cooler regions of the plasma where conditions favor molecular recombination. Plasma plume persistence was shown to increase with the reduction of O_2 PPs. Segregation in the emitting regions of U atoms and molecules is observed for all O_2 PPs, albeit at various times. For example, the segregation between the distribution of U atoms and U monoxide species is more apparent at later times of plasma evolution with lower O_2 PPs. At higher O_2 PPs, significant variation in plume morphology is seen for UO species, which can be related to higher oxide (U_xO_y) formation further from the target, thereby increasing the likelihood of plume instabilities. Results presented here highlight the complex plasma-chemical interaction between the U plume and the oxygen-containing ambient and provide insight into the spatial characteristics of molecular formation in a laser-produced U plasma.

Conflicts of interest

There are no conflicts to declare.

Acknowledgements

DOE/NNSA Office of Nonproliferation and Verification Research and Development (NA-22). Pacific Northwest National Laboratory is operated for the U.S. DOE by Battelle Memorial

Institute under Contract No. DE-AC05-76RLO1830. Consortium for Verification Technology under Department of Energy National Nuclear Security Administration (DE- NA0002534). National Science Foundation Graduate Research Fellowship Program (DGE 1256260).

References

1. D. LaGraffe, in *Handbook of Security Science*, ed. A. J. Masys, Springer International Publishing, Cham, 2018, DOI: 10.1007/978-3-319-51761-2_18-1, pp. 1-34.
2. C. A. Barrett, W. Chouyyok, R. J. Speakman, K. B. Olsen and R. S. Addleman, *Talanta*, 2017, **173**, 69-78.
3. A. Devaraj, E. Kautz, L. Kovarik, S. Jana, N. Overman, C. Lavender and V. V. Joshi, *Scripta Materialia*, 2018, **156**, 70-74.
4. C. G. Bathke, B. B. Ebbinghaus, B. A. Collins, B. W. Sleaford, K. R. Hase, M. Robel, R. K. Wallace, K. S. Bradley, J. R. Ireland, G. D. Jarvinen, M. W. Johnson, A. W. Prichard and B. W. Smith, *Nuclear Technology*, 2012, **179**, 5-30.
5. E. J. Kautz, D. E. Burkes, V. V. Joshi, C. Lavender and A. Devaraj, *Scientific Reports*, 2019, **in-press**.
6. M. R. Savina, R. Trappitsch, A. Kucher and B. H. Isselhardt, *Analytical Chemistry*, 2018, **90**, 10551-10558.
7. K. R. Campbell, N. R. Wozniak, J. P. Colgan, E. J. Judge, J. E. Barefield, D. P. Kilcrease, M. P. Wilkerson, K. R. Czerwinski and S. M. Clegg, *Spectrochimica Acta Part B: Atomic Spectroscopy*, 2017, **134**, 91-97.
8. S. S. Harilal, B. E. Brumfield, N. Glumac and M. C. Phillips, *Optics Express*, 2018, **26**, 20319-20330.
9. C. Kimblin, R. Trainham, G. A. Capelle, X. L. Mao and R. E. Russo, *Aip Adv*, 2017, **7**, 095208.
10. S. S. Harilal, B. E. Brumfield, N. L. LaHaye, K. C. Hartig and M. C. Phillips, *Applied Physics Reviews*, 2018, **5**, 021301.
11. L. A. Finney, P. J. Skrodzki, M. Burger, J. Nees, S. S. Harilal and I. Jovanovic, *Optics Letters*, 2019, **44**, 2783-2786.
12. M. C. Phillips, B. E. Brumfield, N. L. LaHaye, S. S. Harilal, K. C. Hartig and I. Jovanovic, *Scientific Reports*, 2017, **7**, 3784.
13. L. Kaledin and M. Heaven, *Journal of Molecular Spectroscopy*, 1997, **185**, 1-7.
14. L. A. Kaledin, J. E. Mccord and M. C. Heaven, *Journal of Molecular Spectroscopy*, 1994, **164**, 27-65.
15. M. S. Finko and D. Curreli, *Physics of Plasmas*, 2018, **25**, 083112.
16. P. J. Skrodzki, M. Burger, I. Jovanovic, M. C. Phillips, B. E. Brumfield and S. S. Harilal, *Optics Letters*, 2018, **43**, 5118-5121.
17. D. G. Weisz, J. C. Crowhurst, W. J. Siekhaus, T. P. Rose, B. Koroglu, H. B. Radousky, J. M. Zaug, M. R. Armstrong, B. H. Isselhardt, M. K. Savina, M. Azer, M. S. Finko and D. Curreli, *Applied Physics Letters*, 2017, **111**, 034101.
18. X. Mao, G. C.-Y. Chan, I. Choi, V. Zorba and R. E. Russo, *J. Radioanal. Nucl. Chem.*, 2017, **312**, 121-131.
19. K. C. Hartig, S. S. Harilal, M. C. Phillips, B. E. Brumfield and I. Jovanovic, *Optics Express*, 2017, **25**, 11477-11490.
20. P. J. Skrodzki, N. P. Shah, N. Taylor, K. C. Hartig, N. L. LaHaye, B. E. Brumfield, I. Jovanovic, M. C. Phillips and S. S. Harilal, *Spectrochimica Acta Part B: Atomic Spectroscopy*, 2016, **125**, 112-119.
21. D. G. Weisz, J. C. Crowhurst, M. S. Finko, T. P. Rose, B. Koroglu, R. Trappitsch, H. B. Radousky, W. J. Siekhaus, M. R. Armstrong, B. H. Isselhardt, M. Azer and D. Curreli, *The Journal of Physical Chemistry A*, 2018, **122**, 1584-1591.
22. D. Zhang, X. Ma, S. Wang and X. Zhu, *Plasma Science and Technology*, 2015, **17**, 971-974.
23. M. S. Finko, D. Curreli, D. G. Weisz, J. C. Crowhurst, T. P. Rose, B. Koroglu, H. B. Radousky and M. R. Armstrong, *Journal of Physics D: Applied Physics*, 2017, **50**, 485201.
24. T. Dietz, P. Kohns and G. Ankerhold, *Spectrochimica Acta Part B: Atomic Spectroscopy*, 2018, **148**, 51-59.
25. I. B. Gornushkin and U. Panne, *Spectrochimica Acta Part B: Atomic Spectroscopy*, 2010, **65**, 345-359.
26. I. B. Gornushkin, S. V. Shabanov, N. Omenetto and J. D. Winefordner, *Journal of Applied Physics*, 2006, **100**, 073304.
27. T. E. Itina, J. Hermann, P. Delaporte and M. Sentis, *Physical Review E*, 2002, **66**, 066406.
28. S. Noël, J. Hermann and T. Itina, *Applied Surface Science*, 2007, **253**, 6310-6315.
29. M. Ullmann, S. K. Friedlander and A. Schmidt-Ott, *Journal of Nanoparticle Research*, 2002, **4**, 499-509.
30. H. J. Kunze, *Introduction to Plasma Spectroscopy* Springer, Heidelburg, 2009.
31. H. Niki, T. Yasuda and I. Kitazima, *Journal of Nuclear Science and Technology*, 1998, **35**, 34-39.
32. K. C. Hartig, I. Ghebregziabher and I. Jovanovic, *Scientific Reports*, 2017, **7**, 43852.
33. S. S. Harilal, B. E. Brumfield, B. D. Cannon and M. C. Phillips, *Analytical chemistry*, 2016, **88**, 2296-2302.
34. P. Ran, H. Hou and S.-N. Luo, *Journal of Analytical Atomic Spectrometry*, 2017, **32**, 2254-2262.
35. R. Glaus, J. Riedel and I. Gornushkin, *Analytical Chemistry*, 2015, **87**, 10131-10137.
36. K. F. Al-Shboul, S. M. Hassan and S. S. Harilal, *Plasma Sources Science and Technology*, 2016, **25**, 065017.
37. K. K. Anoop, M. P. Polek, R. Bruzzese, S. Amoruso and S. S. Harilal, *Journal of Applied Physics*, 2015, **117**, 083108.
38. S. Gurlui, M. Agop, P. Nica, M. Ziskind and C. Focsa, *Physical Review E*, 2008, **78**, 026405.
39. S. S. Harilal, P. K. Diwakar, M. P. Polek and M. C. Phillips, *Optics Express*, 2015, **23**, 15608-15615.
40. J. Siegel, G. Epurescu, A. Perea, F. J. Gordillo-Vázquez, J. Gonzalo and C. N. Afonso, *Optics letters*, 2004, **29**, 2228-2230.
41. N. Farid, S. Harilal, H. Ding and A. Hassanein, *Journal of applied physics*, 2014, **115**, 033107.
42. S. S. Harilal, E. J. Kautz, B. E. Bernacki, P. J. Skrodzki, M. Burger, M. C. Phillips and I. Jovanovic, *Physical Chemistry Chemical Physics*, 2019, **21**, 16161-16169.
43. P. J. Skrodzki, M. Burger, I. Jovanovic, M. C. Phillips, J. Yeak, B. E. Brumfield and S. S. Harilal, *Physics of Plasmas*, 2019, **26**, 083508.
44. S. S. Harilal, C. V. Bindhu, M. S. Tillack, F. Najmabadi and A. C. Gaeris, *J. Appl. Phys.*, 2003, **93**, 2380-2388.
45. M. Capitelli, A. Casavola, G. Colonna and A. De Giacomo, *Spectrochimica Acta Part B: Atomic Spectroscopy*, 2004, **59**, 271-289.
46. S. V. Shabanov and I. B. Gornushkin, *Applied Physics A*, 2015, **121**, 1087-1107.
47. K. Rifai, F. Vidal and T. W. Johnston, *Phys Plasmas*, 2007, **14**, 082311.